Strain-Induced Effects on the Degenerate Spectral Line of Chromium in MgO Crystals*

A. L. SCHAWLOW, A. H. PIKSIS,† AND S. SUGANO‡
Bell Telephone Laboratories, Inc., Murray Hill, New Jersey
(Received January 26, 1961)

When uniaxial pressure is applied along [100], [110], and [111] directions to MgO crystals with chromium impurities, both a splitting and a shift of the purely cubic field fluorescence line at 14 319 cm^{-1} are observed. The splitting is ascribed to the removal of the degeneracy associated with the $t_2^3\,{}^2E$ excited state by the strain-induced low-symmetry crystal fields. A theoretical calculation of the splitting, assuming a point-charge model, gives a surprisingly good agreement with the experiment. The shift is clearly due to the isotropic part of the strain-induced crystal fields, and a simple consideration shows that the observed red shift is caused by the strain-induced change of the Coulomb interaction between the t_2 electrons. Finally, limitations of the point-charge model adopted here are discussed.

1. INTRODUCTION

A TRIVALENT chromium ion in a strong crystalline field of perfect cubic symmetry has degenerate energy levels. The lowest level is the $^4A_2$, an orbital singlet. About 14 400 cm^{-1} above it lies the ^2E level, which has a twofold orbital degeneracy. The transition between these two levels gives rise to a single sharp resonance line, which may be observed in absorption or fluorescence.

If the surrounding octahedron is distorted, the degeneracy other than the Kramers degeneracy is lifted and the ^2E level is split by an amount that depends on the kind and magnitude of the distortion. Thus, in ruby, this splitting is 29 cm^{-1}, while in gallium oxide,[1] it is 158 cm^{-1}.

A distortion of the octahedral field also splits the ground state but by a much smaller amount. The corresponding ground-state splittings in ruby and gallium oxide[2] are, respectively, 0.38 and 1.18 cm^{-1}. These small splittings are not surprising since the $^4A_2$ state is an orbital singlet.

To achieve a better understanding of these crystal field splittings, we have investigated theoretically and experimentally the effects of slightly distorting, in various symmetries, an initially perfect cubic array of negative and positive charges. The base material is magnesium oxide. It has the rocksalt structure, whose simplicity is an advantage in the theoretical analysis. Cr^{3+} ions enter into the lattice as direct substitutes for Mg^{2+} ions. Of course, the extra positive charge of the chromium ion must be compensated somehow, but microwave studies[3,4] have shown that a large fraction of the ions do not have their charge compensation nearby, and so are in fields of good cubic symmetry. These chromium ions give rise to the R line at 6981 A, while compensated ions produce a spectrum of satellite lines farther to the red. We consider here the effects on the R line, which arises from ions initially in cubic sites.[5]

Distortions of the lattice are produced by squeezing the crystal along one of its symmetry axes. When a stress is applied, the line is observed to split because of the splitting of the ^2E state. The splitting of the ground $^4A_2$ state is expected to be very much less, and this is confirmed by recent microwave experiments.[6] We are thus justified in attributing the observed line splitting to the ^2E state.

This experiment differs in an important way from recent investigations of effects of stress on rare earth spectra by Kaplyanskii.[7] In our experiments we observe optically for the first time a stress-induced splitting in the levels of a single ion. In Kaplyanskii's investigation an apparent splitting was observed, which is attributed to different shifts of the energy levels of charge complexes with different orientations in the crystal lattice. Splittings of the individual rare-earth ion levels were too small to observe.

Apparent splittings of the Kaplyanskii type may be observed in MgO with spectral lines originating from Cr^{3+} ions in noncubic sites. A study of the effect of stress on these lines will be helpful in identifying the local site symmetry, and in understanding the mechanisms of charge compensation. However, the study of the noncubic sites has been deferred until the stress-induced splittings of cubic sites were understood.

2. EXPERIMENTAL PROCEDURE AND RESULTS

For the experiments, transparent colorless single crystals of MgO, containing less than ten chromium

* A preliminary account of this work was presented at a meeting of the American Physical Society, November 25, 1960 [Bull. Am. Phys. Soc. **5**, 415 (1960)].

† Present address: Department of Physics, Johns Hopkins University, Baltimore, Maryland.

‡ On leave from Department of Physics, University of Tokyo, Tokyo, Japan.

[1] O. Deutschbein, Ann. Physik. **20**, 828 (1934).

[2] M. Peter and A. L. Schawlow, Bull. Am. Phys. Soc. **5**, 158 (1960).

[3] J. E. Wertz and P. Auzins, Phys. Rev. **106**, 484 (1957).

[4] W. Low, Phys. Rev. **105**, 801 (1957).

[5] S. Sugano, A. L. Schawlow, and F. Varsanyi, Phys. Rev. **120**, 2045 (1960).

[6] Private communications from G. Feher and E. Rosenwasser, J. E. Wertz and P. Auzins, and G. D. Watkins.

[7] A. A. Kaplyanskii, Optics and Spectroscopy **7**, 406, 409 (1959).

ions per million Mg^{2+} ions, are used. From this material, small elongated prisms with smooth polished faces parallel to (001), (110), and (111) crystal planes, respectively, are prepared in part by cleaving, in part by cutting with a diamond wheel to appropriate angles. The longest dimension of each prism is about 10 mm, while the cross-sectional area perpendicular to this direction varies from 1.4 to 6.0 mm^2.

For studying the effect of static uniform uniaxial compression upon the fluorescence radiation originating in the $t_2^3\,{}^4E \rightarrow t_2^3\,{}^4A_2$ transition of the chromium ions, the crystals are properly oriented with respect to their faces and placed in the press, the cut-away view of which is shown in Fig. 1. By placing weights on the loading platform of the press, the uniaxial compressive stress applied to the crystal can be varied from zero to a maximum limited by the stress at which the crystal prism breaks. Thus we have investigated experimentally the cases when the stress is perpendicular to the (001), (110), and (111) crystal planes, respectively. At all times the crystal is directly immersed in liquid nitrogen so that all the experimental data reported here are those attained at 77°K.

The fluorescence of this red line (14 319 cm^{-1}) of a $MgO:Cr^{3+}$ single crystal is excited by a Sylvania Tru-flector low-voltage lamp. In order for it to act as coolant and optical filter, a saturated aqueous solution of cupric sulfate is circulated in a thick layer all around the outside of the Dewar tip which contains the crystal in a liquid-nitrogen bath. As a blue-green filter, transmitting the radiation in the broad-band absorption region of chromium, the cupric sulfate solution is found to be very effective when close to its boiling temperature, at which time its concentration is the highest. A red filter on the entrance slit of the spectrograph cuts out the exciting radiation. The crystal is observed in a direction perpendicular to the applied stress.

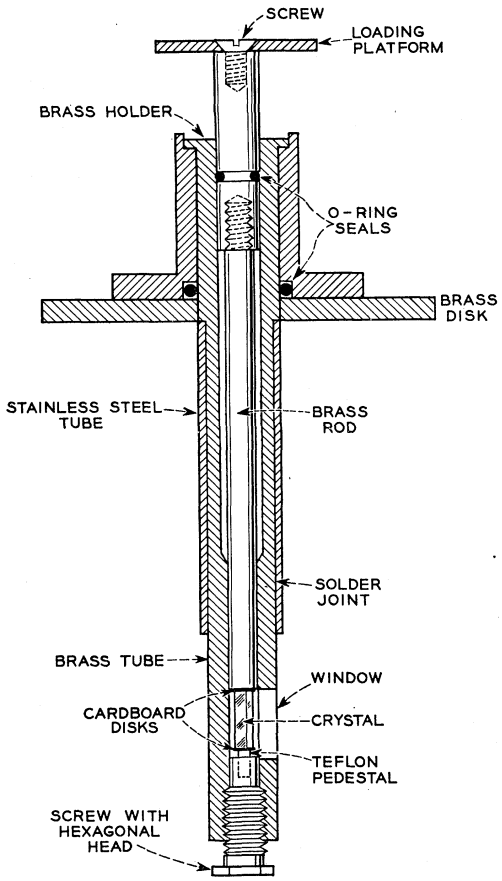

FIG. 1. Apparatus for observing fluorescence of the crystals under uniaxial stress.

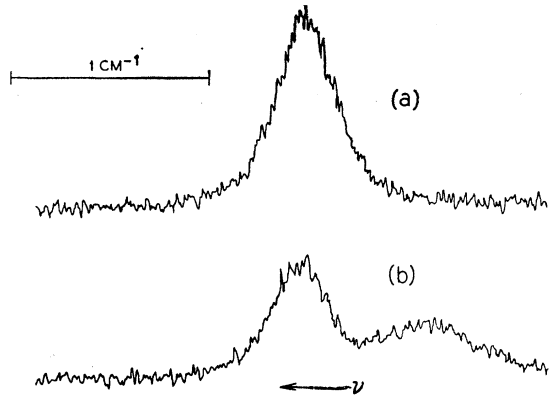

FIG. 2. (a) Spectrometer recording of $MgO:Cr^{3+}$ fluorescence line at 14 319 cm^{-1}. (b) Same line when crystal is subjected to a stress of 11 kg/mm^2 along the [100] direction.

The fluorescent light from the crystal specimen is investigated in two polarizations, parallel and perpendicular to the direction of the applied stress. In all cases, the stress is applied parallel to the entrance slit of the spectrograph.

The spectrum is scanned photoelectrically with a high-resolution vacuum Ebert-type spectrograph, with a focal length of 2 m, manufactured by the Jarrell-Ash Company on the original design by Fastie, Crosswhite, and Gloersen.[8] Equipped with a good replica of a Harrison grating having 7500 lines/in., this instrument provides spectral resolution of about 1/30 cm^{-1} in the region of interest. A carefully designed grating drive gives high wavelength accuracy so that the errors in the wave numbers should not exceed a few times 0.01 cm^{-1}. The detector is an RCA type 7102, S-20, electron photomultiplier tube, immersed in liquid nitrogen. The dispersion of the spectrogram is determined by calibrating the instrument with radiations of known wavelengths from commercial Osram lamps. Then it is possible to find the position of the line in the spectrum, establish the shifts of the intensity peaks, and study line shapes.

Figure 2 shows typical spectrometer recordings. In Fig. 2(a), no stress is applied, while in Fig. 2(b), a

[8] W. G. Fastie, H. M. Crosswhite, and P. Gloersen, J. Opt. Soc. Am. 48, 106 (1958).

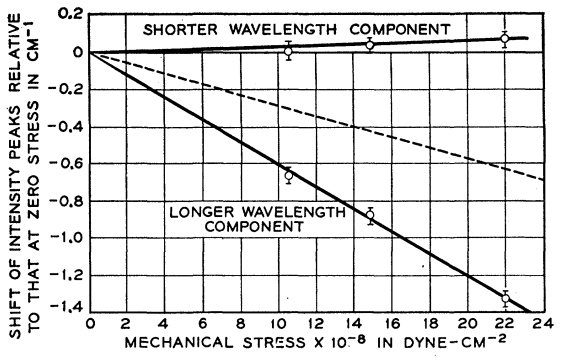

FIG. 3. Splitting and displacement of the line with stress along the [100] direction.

stress of 11 kg/mm² is applied parallel to a [100] direction.

Figures 3–5 show the displacements of the components into which the line splits under increasing stresses along the [100], [110], and [111] directions, respectively. The broken lines in these figures indicate the average displacement. Since the split components have the same degeneracy, a simple average is shown.

In comparison with most other spectral lines in solids, the chromium lines in MgO are quite sharp, having a width of about 0.25 cm^{-1} at low temperatures. However, this width is not caused by the lifetime of the excited state, which is some milliseconds. These experiments show that the linewidth could easily be caused by internal strains, which are always present in these refractory crystals. Indeed, an effective strain of 2×10^{-4} along a [100] direction can cause a splitting equal to the linewidth. A similar internal stress is also found to explain the microwave linewidths of some transition metal ground-state levels in the experiments of Feher and Rosenwasser.[6] It seems likely, therefore, that the linewidths are predominantly due to strain, and would be less in more perfect crystals.

3. THEORETICAL PRELIMINARIES

A. Stress and Strain

In our experiments, the applied stress P ($P<0$) is *simple pressure*,[9] normal to the (001), (110), and (111) planes. Therefore, the independent stress components referred to axes x, y, z are given for each case as follows:

Case (i). Simple pressure $\perp$ (001):

$$Z_z=P, \quad X_x=Y_y=Y_z=Z_x=X_y=0; \tag{3.1}$$

Case (ii). Simple pressure $\perp$ (110):

$$X_x=Y_y=X_y=P/2, \quad Z_z=Y_z=Z_x=0; \tag{3.2}$$

Case (iii). Simple pressure $\perp$ (111):

$$X_x=Y_y=Z_z=Y_z=Z_x=X_y=P/3. \tag{3.3}$$

In stress components, the capital letter indicates the direction of force and the script indicates the normal to the plane to which the force is applied.

Then, strain components are given as follows:

Case (i). $e_{xx}=e_{yy}=s_{12}P, \quad e_{zz}=s_{11}P,$ (3.4)
$e_{yz}=e_{zx}=e_{xy}=0;$

Case (ii). $e_{xx}=e_{yy}=(s_{11}+s_{12})P/2, \quad e_{zz}=s_{12}P,$ (3.5)
$e_{yz}=e_{zx}=0, \quad e_{xy}=s_{44}P/2;$

Case (iii). $e_{xx}=e_{yy}=e_{zz}=(s_{11}+2s_{12})P/3,$ (3.6)
$e_{yz}=e_{zx}=e_{xy}=s_{44}P/3;$

where s_{ij}'s are elastic compliance factors and, in cubic crystals, they are related to stiffness constant c_{ij} in the following way[10]:

$$\begin{aligned} s_{11}&=(c_{11}+c_{12})/(c_{11}-c_{12})(c_{11}+2c_{12});\\ s_{12}&=-c_{12}/(c_{11}-c_{12})(c_{11}+2c_{12});\\ s_{44}&=1/c_{44}. \end{aligned} \tag{3.7}$$

For discussing distortions of cubic crystals, it is sometimes more convenient to use strain components designated by cubic irreducible representation such as $e(A_1)$, $e_u(E)$, $e_v(E)$, $e_\xi(T_2)$, $e_\eta(T_2)$, and $e_\zeta(T_2)$, instead of using six independent strain components e_{xx}, e_{yy}, e_{zz}, e_{xy}, e_{yz}, and e_{zx}. The new strain components $e_\gamma(\Gamma)$ are given by

$$\begin{aligned} e(A_1)&=e_{xx}+e_{yy}+e_{zz}, & e_\xi(T_2)&=e_{yz},\\ e_u(E)&=2e_{zz}-e_{xx}-e_{yy}, & e_\eta(T_2)&=e_{zx},\\ e_v(E)&=e_{xx}-e_{yy}, & e_\zeta(T_2)&=e_{xy}, \end{aligned} \tag{3.8}$$

which transform in the same way as the basis of the irreducible representation $\varphi(\Gamma\gamma)$ under the operations of the octahedral group. Therefore, $e(A_1)$ gives spherically symmetric and cubic distortions; $e_u(E)$, axial and tetragonal distortions around the z axis; $e_v(E)$, rhombic distortions preserving mirror reflection as to the vertical plane passing through x or y axis; $e_\zeta(T_2)$, rhombic

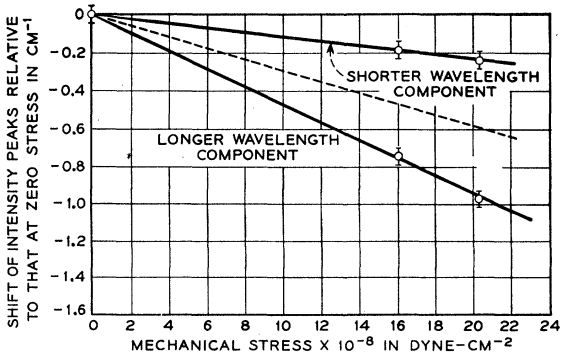

FIG. 4. Splitting and displacement of the line with stress along the [110] direction.

[9] A. E. H. Love, *A Treatise on the Mathematical Theory of Elasticity* (Cambridge University Press, New York, 1927), 4th ed., Chap. 3.

[10] C. Kittel, *Introduction to Solid State Physics* (John Wiley & Sons, Inc., New York, 1954), 2nd ed., Chap. 4, p. 91.

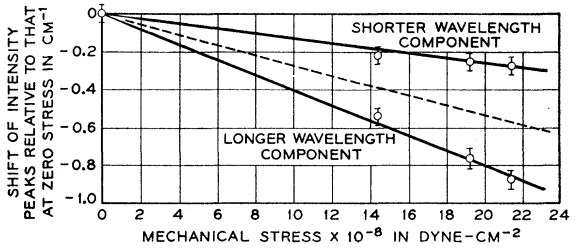

FIG. 5. Splitting and displacement of the line with stress along the [111] direction.

distortions preserving mirror reflection as to the vertical plane passing through $x=y$ or $x=-y$ lines; $[e_\xi(T_2)+e_\eta(T_2)+e_\zeta(T_2)]/\sqrt{3}$, under the condition $e_\xi(T_2)=e_\eta(T_2)=e_\zeta(T_2)$, trigonal distortions around the trigonal axis of the octahedron; and so on.

Equations (3.4)–(3.6) are expressed in terms of these strain components as follows:

Case (i).

$$\begin{aligned} &e(A_1)=(s_{11}+2s_{12})P,\\ &e_u(E)=2(s_{11}-s_{12})P,\\ &e_v(E)=e_\xi(T_2)=e_\eta(T_2)=e_\zeta(T_2)=0; \end{aligned} \tag{3.9}$$

Case (ii).

$$\begin{aligned} &e(A_1)=(s_{11}+2s_{12})P,\\ &e_u(E)=-(s_{11}-s_{12})P,\\ &e_v(E)=e_\xi(T_2)=e_\eta(T_2)=0,\\ &e_\zeta(T_2)=s_{44}P/2; \end{aligned} \tag{3.10}$$

Case (iii).

$$\begin{aligned} &e(A_1)=(s_{11}+2s_{12})P,\\ &e_u(E)=e_v(E)=0,\\ &e_\xi(T_2)=e_\eta(T_2)=e_\zeta(T_2),\\ &[e_\xi(T_2)+e_\eta(T_2)+e_\zeta(T_2)]/\sqrt{3}=s_{44}P/\sqrt{3}. \end{aligned} \tag{3.11}$$

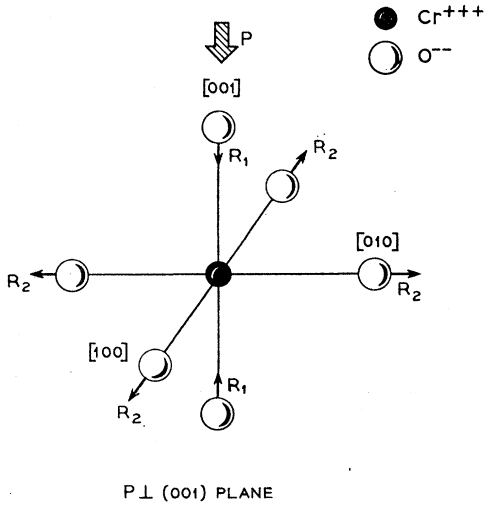

FIG. 6. Displacements of six neighboring oxygen ions by stress along the [001] direction. The upper and lower oxygen ions move inward by R_1; the others move outward by R_2.

Thus we can easily know symmetries of the distortion induced by the stress. In Figs. 6–8, displacements of the six nearest-neighbor oxygen ions relative to the central chromium ion are described for our three cases.

B. Induced Crystal Field Change

From symmetry considerations, it is easily seen that the strain-induced change of the crystal field V, which is linear as to the strain, can be written in the form

$$V=\sum_{\Gamma\gamma} C_\gamma(\Gamma)V_\gamma(\Gamma)e_\gamma(\Gamma), \tag{3.12}$$

where $\Gamma\gamma$ runs over A_1e_1, Eu, Ev, $T_2\xi$, $T_2\eta$, and $T_2\zeta$. $V_\gamma(\Gamma)$ is a function of electron coordinates and has the same transformation property as that of $e_\gamma(\Gamma)$. $C_\gamma(\Gamma)$ is a constant. If $V_\gamma(\Gamma)$ is expanded in a power series of electron coordinates, it is further written as

$$C_\gamma(\Gamma)V_\gamma(\Gamma)=\sum_n C_{n,\gamma}(\Gamma)V_{n,\gamma}(\Gamma), \tag{3.13}$$

where $C_{n,\gamma}(\Gamma)$ is a constant, and $V_{n,\gamma}(\Gamma)$ is a normalized *cubic harmonics*[11] with the $\Gamma\gamma$ symmetry multiplied by r^n. When the crystal field is acting on d electrons, n in Eq. (3.13) runs up to 4. Then, the explicit forms of $V_{n,\gamma}(\Gamma)$ are given as follows:

$$\begin{aligned} &V_4(A_1)=r^4\left(\frac{1}{\sqrt{12}}\right)\left[(\sqrt{7})Y_{40}+(\sqrt{5})\frac{1}{\sqrt{2}}(Y_{44}+Y_{4-4})\right],\\ &V_{2,u}(E)=r^2Y_{20},\\ &V_{4,u}(E)=r^4\left(\frac{1}{\sqrt{12}}\right)\left[(\sqrt{5})Y_{40}-(\sqrt{7})\frac{1}{\sqrt{2}}(Y_{44}+Y_{4-4})\right],\\ &V_{2,v}(E)=r^2\left(\frac{1}{\sqrt{2}}\right)(Y_{22}+Y_{2-2}),\\ &V_{4,v}(E)=r^4\left(\frac{1}{\sqrt{2}}\right)(Y_{42}+Y_{4-2}),\\ &V_{2,\xi}(T_2)=r^2\left(\frac{i}{\sqrt{2}}\right)(Y_{21}+Y_{2-1}),\\ &V_{4,\xi}(T_2)=r^4\left(\frac{1}{\sqrt{8}}\right)\left[\frac{i}{\sqrt{2}}(Y_{41}+Y_{4-1})-(\sqrt{7})\frac{i}{\sqrt{2}}(Y_{43}+Y_{4-3})\right],\\ &V_{2,\eta}(T_2)=r^2\left(-\frac{1}{\sqrt{2}}\right)(Y_{21}-Y_{2-1}),\\ &V_{4,\eta}(T_2)=r^4\left(\frac{1}{\sqrt{8}}\right)\left[\frac{1}{\sqrt{2}}(-Y_{41}+Y_{4-1})+(\sqrt{7})\frac{1}{\sqrt{2}}(-Y_{43}+Y_{4-3})\right], \end{aligned} \tag{3.14}$$

[11] H. A. Bethe, Ann. Physik **3**, 133 (1929).

$$V_{2,\xi}(T_2)=r^2\left(-\frac{i}{\sqrt{2}}\right)(Y_{22}-Y_{2-2}),$$

$$V_{4,\xi}(T_2)=r^4\left(\frac{i}{\sqrt{2}}\right)(-Y_{42}+Y_{4-2}),$$

where $Y_{lm}=\Theta(lm)\Phi(m)$ are spherical harmonics defined by Condon and Shortley.[12]

The calculation of the coefficients $C_{n,\gamma}(\Gamma)$ involves the same difficulties as encountered in the calculation of cubic crystal field strengths. However, it is possible to get the values of the coefficients, when we use the point-charge model and sum up appropriately the electrostatic field coming from the positive and negative charges at all the lattice points. Such a calculation has been done by Kanamori,[13] and our coefficients are related to his coefficients,[14] A_1, C_1, D_1, F_1, and H_1 in the following ways:

$$C_4(A_1)=\left(\frac{8\sqrt{\pi}}{5\sqrt{21}}\right)\left(D_1+\frac{7}{3}F_1\right),$$

$$C_{2,u}(E)=\left(\frac{2\sqrt{\pi}}{\sqrt{5}}\right)A_1,\quad C_{4,u}(E)=\left(\frac{4\sqrt{\pi}}{3\sqrt{15}}\right)F_1,$$

$$C_{2,v}(E)=\left(\frac{2\sqrt{3\pi}}{\sqrt{5}}\right)A_1,\quad C_{4,v}(E)=-\left(\frac{4\sqrt{\pi}}{3\sqrt{15}}\right)F_1, \quad (3.15)$$

$$C_{2,\xi}(T_2)=C_{2,\eta}(T_2)=C_{2,\zeta}(T_2)=\left(\frac{2\sqrt{\pi}}{\sqrt{15}}\right)C_1,$$

$$C_{4,\xi}(T_2)=C_{4,\eta}(T_2)=C_{4,\zeta}(T_2)=-\left(\frac{4\sqrt{\pi}}{3\sqrt{5}}\right)H_1.$$

In the following discussion, we will use Eq. (3.15) together with Kanamori's numerical values. Propriety of using the point-charge model will be discussed later.

C. Splitting of the $t_2^3\ ^2E$ State

Now we study splitting of the degenerate $t_2^3\ ^2E$ level, which is responsible for the fluorescence line examined here, in three cases.

Case (i)

As (3.9) shows, the distortion is of tetragonal symmetry around z axis. Detailed examination shows that, for the real system with reasonable strengths of the cubic field, Coulomb interaction, and spin-orbit interaction, the configuration mixing among the ^2E states plays the predominant role in giving the splitting; the splitting is given in good approximation by

$$W(^2E\pm\tfrac{1}{2}v)-W(^2E\pm\tfrac{1}{2}u)=[b^2\sum_{n=2,4}C_{n,u}(E)\,(e\|V_n(E)\|e)+(8\sqrt{3}bc/6)\sum_{n=2,4}C_{n,u}(E)\,(t_2\|V_n(E)\|t_2)]e_u(E), \quad (3.16)$$

where b and c are the coefficients of the configuration mixing defined as follows[15]:

$$\Psi(\text{lowest }^2E)=a\Psi(t_2^3\ ^2E)+b\Psi(t_2^2(^1A_1)e\ ^2E)+c\Psi(t_2^2(^1E)e\ ^2E). \quad (3.17)$$

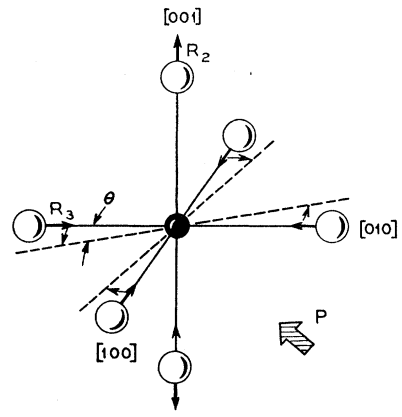

FIG. 7. Displacements of six neighboring oxygen ions by stress along the [110] direction. The upper and lower oxygen ions move outward by R_2; the others move inward by R_3. The angle θ is in the (001) plane.

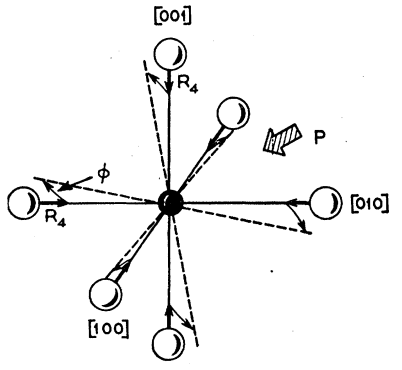

FIG. 8. Displacements of the neighboring oxygen ions by stress along the [111] direction. All the oxygen ions move inward by R_4. The angles ϕ are in such directions that two upper and lower triangles, whose apexes are, respectively, on the sets of (x,y,z) and $(-x,-y,-z)$ axes, are squeezed toward each other, preserving the trigonal symmetry around the [111] axis. Throughout Figs. 6–8, if $P=-22\times10^8$ d cm^{-2} is assumed, we have $R_1=1.79\times10^{-3}A$, $R_2=0.40\times10^{-3}A$, $R_3=(R_1-R_2)/2$, $R_4=(R_1-2R_2)/3$, $\theta=2.1\times10^{-2}$ deg, and $\phi=\sqrt{2}\theta/3$.

[12] E. U. Condon and G. H. Shortley, *The Theory of Atomic Spectra* (Cambridge University Press, New York, 1935), Chap. 3, p. 51.

[13] J. Kanamori, Progr. Theoret. Phys. (Kyoto) **17**, 197 (1956).

[14] $A_1=-5.96R^{-3}$, $C_1=11.93R^{-3}$, $F_1=-16.61R^{-5}$, and $H_1=10.21R^{-5}$. R is the lattice constant in atomic units.

[15] S. Sugano and M. Peter (to be published).

The double-barred matrices[16] are given by

$$(e\|V_n(E)\|e)=-2(eu|V_{n,u}(E)|eu)$$
$$=\begin{cases}-[(2\sqrt{5})/(7\sqrt{\pi})]\langle r^2\rangle & \text{for } n=2,\\ -[(3\sqrt{5})/(7\sqrt{3\pi})]\langle r^4\rangle & \text{for } n=4;\end{cases} \quad (3.18)$$

$$(t_2\|V_n(E)\|t_2)=\sqrt{3}(t_2\zeta|V_{n,u}(E)|t_2\zeta)$$
$$=\begin{cases}[(\sqrt{15})/(7\sqrt{\pi})]\langle r^2\rangle & \text{for } n=2,\\ [(\sqrt{5})/(7\sqrt{\pi})]\langle r^4\rangle & \text{for } n=4.\end{cases} \quad (3.19)$$

The other term, which comes next to Eq. (3.16) in giving the splitting, is the third-order perturbation $V_{so}\,\Delta V\,V_{so}$ (V_{so}=spin-orbit interaction (ΔV=strain-induced crystal field), in which both the intermediate states are the $t_2^2e\,^4T_2$ state, but it is found negligible compared to Eq. (3.16).

Case (ii)

We have both tetragonal and rhombic distortions in this case, as Eq. (3.10) shows. The magnitude of the tetragonal distortion is just half the previous one and the sign is reversed. The splitting due to the rhombic distortion is found to come mainly from the second-order perturbation $V_{so}\,\Delta V+\Delta V\,V_{so}$ in which the intermediate state is the $t_2^3\,^2T_2$ state. Furthermore, this distortion mixes the u and v components of the ^2E state.

The resultant energy matrix of the ^2E state for both these distortions is given by

	$\pm\frac{1}{2},u$	$\pm\frac{1}{2},\mp iv$
$\pm\frac{1}{2},u$	α	β
$\pm\frac{1}{2},\mp iv$	β	$-\alpha$

(3.20)

where α and β come from the tetragonal and rhombic distortions, respectively, and they are given as follows:

$$\alpha=\tfrac{1}{4}\{[W(^2Ev)-W(^2Eu)] \text{ of Eq. (3.16)}\},$$

$$\beta=\frac{\sqrt{2}}{3}\zeta e_{xy}\sum_{n=2,4}C_{n,\xi}(T_2)(t_2\|V_n(T_2)\|t_2)/[W(t_2^3\,^2T_2)-W(t_2^3\,^2E)],$$
$$(\alpha<0,\quad \beta<0 \quad \text{for} \quad P<0). \quad (3.21)$$

In Eq. (3.21) the factor ζ is a constant of the spin-orbit interaction for a t_2-electron and the double-barred matrices are given by

$$(t_2\|V_n(T_2)\|t_2)=(\sqrt{6})(t_2\eta|V_{n,\xi}(T_2)|t_2\xi)$$
$$=\begin{cases}[(3\sqrt{10})/(14\sqrt{\pi})]\langle r^2\rangle & \text{for } n=2,\\ [(\sqrt{30})/(7\sqrt{\pi})]\langle r^2\rangle & \text{for } n=4.\end{cases} \quad (3.22)$$

The eigenvalues and eigenvectors of Eq. (3.20) are found to be

$W=(\alpha^2+\beta^2)^{\frac{1}{2}}$:

$$\begin{cases}-\sin\theta\,\Psi(^2E\tfrac{1}{2}u)-i\cos\theta\,\Psi(^2E\tfrac{1}{2}v),\\ -\sin\theta\,\Psi(^2E-\tfrac{1}{2}u)+i\cos\theta\,\Psi(^2E-\tfrac{1}{2}v);\end{cases} \quad (3.23)$$

$W=-(\alpha^2+\beta^2)^{\frac{1}{2}}$:

$$\begin{cases}\cos\theta\,\Psi(^2E\tfrac{1}{2}u)-i\sin\theta\,\Psi(^2E\tfrac{1}{2}v),\\ \cos\theta\,\Psi(^2E-\tfrac{1}{2}u)+i\sin\theta\,\Psi(^2E-\tfrac{1}{2}v);\end{cases} \quad (3.24)$$

where

$$\tan2\theta=\beta/\alpha,\quad 0\leq 2\theta\leq\pi/2. \quad (3.25)$$

In Eqs. (3.20), (3.23), and (3.24), it should be noticed that the magnetic spin quantum number, $M_s=\pm\frac{1}{2}$, is referred to the z axis. For $P>0$, the signs of the eigenvalues should be reversed, keeping the eigenvectors unchanged.

Case (iii)

As Eq. (3.11) shows, only a trigonal distortion is induced in this case. The splitting due to the trigonal distortion has been fully discussed in the case of ruby spectrum.[17] The splitting is expressed approximately by

$$W(^2E\pm\tfrac{1}{2}u_{\pm})-W(^2E\pm\tfrac{1}{2}u_{\mp})=-4K\zeta/[W(t_2^3\,^2T_2)-W(t_2^3\,^2E)], \quad (3.26)$$

where

$$K=-(1/\sqrt{6})e_{xy}\sum_{n=2,4}C_{n,\xi}(T_2)(t_2\|V_n(T_2)\|t_2). \quad (3.27)$$

The double-barred matrices in Eq. (3.27) are already given in Eq. (3.22). Note that the spin in Eq. (3.26) is quantized along the trigonal axis.

D. Polarization

The previous study[5] of the Zeeman effect of the fluorescence line we are examining here has revealed that the fluorescence is magnetic dipole radiation. The polarization of the split components in each case can be calculated in a way similar to that given in that paper. Therefore, without mentioning detailed procedures of the calculation, we shall quote here only the results, which are important in determining the signs of the strain-induced crystal fields from the experimental data.

Case (i)

$$S(^2E\pm\tfrac{1}{2}u)/S(^2E\pm\tfrac{1}{2}v)=\begin{cases}3 & \text{for } H\perp[001]\\ 0 & \text{for } H\|[001],\end{cases} \quad (3.28)$$

where S stands for a dipole strength and H for an oscillating magnetic vector of the radiation.

[16] Y. Tanabe and H. Kamimura, J. Phys. Soc. Japan **13**, 394 (1958).

[17] S. Sugano and Y. Tanabe, J. Phys. Soc. Japan **13**, 880 (1958).

TABLE I. The strain-induced splittings, shifts, and the polarization of the split components. The definitions of the splitting and the polarization are given in Eqs. (4.4), (3.28), (3.29), and (3.30), of the text. Δ and λ are given in cm^{-1} and P in dynes/cm^2 ($P<0$).

Case	Calc split. $\Delta/(-P)$	Obs split. $\Delta/(-P)$	Calc pol.[a]		Obs pol.	Obs shift $\lambda/(-P)$
(i)	6.8 ± 10^{-10}	$(6.3\pm0.2)\times10^{-10}$	σ	3	2.4	2.9×10^{-10}
			π	0	0.4	
(ii)	-3.8×10^{-10}	$-(3.6\pm0.1)\times10^{-10}$	σ_1	1.7	1.2	2.9×10^{-10}
			σ_2	0.05	0.01	
			π	4.6	1.5	
(iii)	-2.0×10^{-10}	$-(2.8\pm0.1)\times10^{-10}$	σ	0.6	0.61	2.6×10^{-10}
			π	3	1.6	

[a] π means the polarization with the magnetic vector of light parallel to the stress (simple pressure), and σ the polarization perpendicular to the stress, σ_1 and σ_2 in Case (ii) distinguishes two kinds of σ in such a way that σ_1: $H\|[1\bar{1}0]$ and σ_2: $H\|[001]$.

Case (ii)

$$S(^2E\pm\tfrac{1}{2}\bar{u})/S(^2E\pm\tfrac{1}{2}\bar{v}) = \begin{cases} (4+2\cos2\theta-\sqrt{3}\sin2\theta)/(4-2\cos2\theta & \\ \quad +\sqrt{3}\sin2\theta) & \text{for } H\|[1\bar{1}0] \\ (4+2\cos2\theta+\sqrt{3}\sin2\theta)/(4-2\cos2\theta & \\ \quad -\sqrt{3}\sin2\theta) & \text{for } H\|[110] \\ \tan^2\theta & \text{for } H\|[001], \end{cases} \tag{3.29}$$

where $(^2E\pm\frac{1}{2}\bar{u})$ and $(^2E\pm\frac{1}{2}\bar{v})$ are the split components given by Eqs. (3.24) and (3.23), respectively, and θ is given by Eq. (3.25).

Case (iii)

$$S(^2E\pm\tfrac{1}{2}u_\pm)/S(^2E\pm\tfrac{1}{2}u_\mp) = \begin{cases} \frac{3}{5} & \text{for } H\perp[111], \\ 3 & \text{for } H\|[111]. \end{cases} \tag{3.30}$$

4. COMPARISON WITH THE EXPERIMENT

In order to obtain numerical values of the splitting theoretically, it is necessary to know the values of the elastic compliance factors or the stiffness constants. The values of the stiffness constants c_{ij} at 77°K are determined from Durand's experimental curves against temperature,[18] displacing them uniformly so as to pass through the points that Bhagavantam[19] determined at room temperature more accurately. The values (in d/cm^2) are as follows:

$$\begin{aligned} c_{11} &= 29.54\times10^{11}, \\ c_{12} &= 8.49\times10^{11}, \\ c_{44} &= 14.99\times10^{11}. \end{aligned} \tag{4.1}$$

The values of $\langle r^2\rangle$ and $\langle r^4\rangle$ appearing in the expressions for the splitting are estimated by using Watson's analytical Hartree-Fock solution for a free Cr^{3+} ion.[20] They are found to be

$$\begin{aligned} \langle r^2/R^2\rangle &= 0.0918, \\ \langle r^4/R^4\rangle &= 0.0179, \\ R &= 3.97 \text{ (a.u.)}. \end{aligned} \tag{4.2}$$

The numerical values of the configuration mixing coefficients, b and c, appearing in Eq. (4.16) are[15]

$$b=1.3\times10^{-1}; \quad c=9.3\times10^{-2}, \tag{4.3}$$

which have been fairly accurately computed for ruby. This is justified by the fact that the optical spectrum of MgO:Cr^{3+} is similar to that of ruby.

Now, from Eqs. (3.16), (3.23), (3.24), and (3.26), the magnitudes of the splitting for three cases are easily obtained. For $[W(t_2^3\,{}^2T_2)-W(t_2^3\,{}^2E)]$, we use the experimental value for ruby, 6000 cm^{-1}. The spin-orbit coupling constant ζ is assumed to be 200 cm^{-1}. α and β in Eq. (3.21) are found to be $1.7\times10^{-10}P$ and $0.86\times10^{-10}P$ (cm^{-1}, for P in d/cm^2). Then $\tan2\theta\doteqdot\frac{1}{2}$. Using this value of θ, the polarization (3.29) is given numerically. Since the splitting is proportional to P, we shall hereafter treat the value of $\Delta/(-P)$, where Δ is the magnitude of the splitting defined as

Case (i)
$$\Delta = W(^2E\pm\tfrac{1}{2}u)-W(^2E\pm\tfrac{1}{2}v),$$
Case (ii)
$$\Delta = W(^2E\pm\tfrac{1}{2}\bar{u})-W(^2E\pm\tfrac{1}{2}\bar{v}), \tag{4.4}$$
Case (iii)
$$\Delta = W(^2E\pm\tfrac{1}{2}u_\pm)-W(^2E\pm\tfrac{1}{2}u_\mp),$$

and P is given in units of dynes/cm^2 and always negative in our case.

The numerical values of $\Delta/(-P)$ and the polarization are given in Table I, together with the experimental ones. The signs of the experimental $\Delta/(-P)$ are determined so as to give qualitative agreement between the observed and calculated polarizations.

It should be noticed that the trigonal field parameter K in case (iii) is positive. This is the opposite sign to the case of ruby, as is to be expected since here the

[18] M. A. Durand, Phys. Rev. **50**, 449 (1936).
[19] S. Bhagavantam, Proc. Indian Acad. Sci. **A41**, 72 (1955).
[20] R. E. Watson, Mass. Inst. Technol., Solid-State and Molecular Theory Group, Tech. Rept. No. 12 (June 15, 1959) (unpublished).

octahedron of oxygen ions is compressed along the [111] direction, while in ruby it is stretched.

The observed shifts λ of the center of the split components are also listed in the form $\lambda/(-P)$ in Table I. It is remarkable that the $\lambda/(-P)$'s in the three cases are almost identical. On the other hand, we observe in Eqs. (3.9), (3.10), and (3.11) that the $e(A_1)$'s are same for three cases. Therefore, it seems clear that the shifts are caused by the strain-induced changes of the spherically symmetric and cubic crystal fields. This point will be further discussed in the next section.

5. DISCUSSION

As Table I shows, the agreement between the calculated and observed splitting is surprisingly good. One might say that the agreement is fortuitous, but the fact that it is uniformly good in all cases seems to suggest something significant. The implication of this fact shall be discussed in the following.

In our calculation, the part which should be exposed to a serious criticism is the calculation of the strain-induced crystal field. A similar calculation was applied to the theory of magnetostriction in FeO and CoO crystals by Kanamori[13] by use of the same point-charge model. He calculated deformations of the crystals in the antiferromagnetic states and found that the point-charge approximation overestimated the coupling constants which appeared in the magnetostriction energy. According to his discussion, the covalency effect, which contributes to the cubic crystal field strength in such a sense to cancel the negative contribution due to the overlap between neighboring electron clouds (imperfect screening of nuclear charge due to the overlap), is less important in calculating crystal field strengths of lower symmetry, and thus the point-charge model gives coupling constants which are too large and which should otherwise be reduced by the sole effect of the electron overlap.

In connection with Kanamori's statement, it would be instructive to estimate the cubic field strength Dq in our case by using the same values of $\langle r^2\rangle$ and $\langle r^4\rangle$ as adopted here: Bethe's formula[11] for Dq immediately gives $Dq=338$ cm^{-1}, which is clearly too small. Therefore, our results for both Dq and crystal field strengths of lower symmetry are merely shifted from Kanamori's in the same direction. This shift seems to come from different ways of calculating $\langle r^2\rangle$ and $\langle r^4\rangle$: He used a Slater wave function for the calculation. If a Slater wave function is used in our case, we obtain

$$\langle r^2/R^2\rangle=0.313, \quad \langle r^4/R^4\rangle=0.144,$$

which are much larger than those given in (4.2) calculated by the use of the Hartree-Fock wave function. The above value of $\langle r^4\rangle$ leads us to a fairly good cubic field strength, $Dq=2720$ cm^{-1}, but it clearly makes the predicted splittings too large. This situation corresponds just to Kanamori's case.

At the present stage, we have no definite knowledge to enable us to determine which better approximates the real wave function in the crystal, the Hartree-Fock or Slater wave function for the free ion. However, it would be of some value to point out the following fact: In the tetragonal splitting, the first and second terms for $n=4$ in Eq. (3.16) almost cancel. Thus the predicted splitting in case (i) is almost independent of the value of $\langle r^4\rangle$. Contrary to this, the splitting in case (iii) is rather sensitive to the relative magnitudes of $\langle r^2\rangle$ and $\langle r^4\rangle$, because the two terms in Eq. (3.27) which are found to be of the same order of magnitude but with the opposite sign. Then, bearing in mind the fact that $\langle r^4\rangle_{\text{Slater}}/\langle r^4\rangle_{\text{H-F}}$ is much larger than $\langle r^2\rangle_{\text{Slater}}/\langle r^2\rangle_{\text{H-F}}$, we expect, when a Slater function is used, discrepancies between the predicted and observed splittings not to be uniformly distributed in all cases. Actually we have $\Delta/(-P)=23\times10^{-10}$ for case (i) and 4×10^{-10} for case (iii).

Considering the above-mentioned discussions, the authors would like to think that Watson's Hartree-Fock wave function is better applicable to our problem than the Slater function. A definite conclusion, however, should be drawn after studies are made on the effects of the imperfect screening of nuclear charges, covalency, deformation of the lattice due to chromium impurities, and polarization due to the excess charge of the impurities, which are ignored in our treatment.

In the previous section, it was mentioned that the shifts of the center of the split components are caused by the strain-induced spherically symmetric and cubic crystal fields. However, detailed examination shows that an increase in strength of the cubic field causes only blue shifts. Therefore, the observed red shifts are explained only by introducing a decrease of the strength of the Coulomb interaction B as the cubic and/or spherically symmetric crystal field increases. This fact has also been observed by Stephens and Drickamer[21] in a NiO crystal applying high isotropic pressure. Quantitative determination of the change of the Coulomb interaction as a function of the isotropic part of the strain is very difficult, because the counteracting contribution, which should be subtracted from the observed shift, is hard to know exactly.

ACKNOWLEDGMENTS

We wish to thank A. M. Clogston, G. E. Devlin, and S. Geschwind for helpful discussions. We are also indebted to Professor H. G. Drickamer, G. Feher, and Mrs. E. Rosenwasser for discussions, and for communicating some of their results before publication.

[21] D. R. Stephens and H. G. Drickamer (to be published).